NeuroImage 115 (2015) 52–63

Contents lists available at ScienceDirect

NeuroImage

journal homepage: www.elsevier.com/locate/ynimg

Sparse, reliable, and long-term stable representation of periodic whisker deflections in the mouse barrel cortex

Johannes M. Mayrhofer [a,c,*], Florent Haiss [a,d,e,f], Fritjof Helmchen [b,c], Bruno Weber [a,c]

[a] Institute of Pharmacology and Toxicology, University of Zurich, CH-8057 Zurich, Switzerland
[b] Brain Research Institute, University of Zurich, CH-8057 Zurich, Switzerland
[c] Neuroscience Center Zurich, CH-8057 Zurich, Switzerland
[d] IZKF Aachen, Medical Faculty of the RWTH Aachen University, D-52062 Aachen, Germany
[e] Institute for Neuropathology, RWTH Aachen University, D-52062 Aachen, Germany
[f] Department of Ophthalmology, RWTH Aachen University, D-52062 Aachen, Germany

ARTICLE INFO

Article history:
Received 20 January 2015
Accepted 21 April 2015
Available online 28 April 2015

Keywords:
Vibrotactile perception
Systems neuroscience
Whisker somatosensory cortex of mouse
In vivo two-photon microscopy
Yellow Cameleon 3.60
Barrel field and in vivo calcium-imaging

ABSTRACT

The rodent whisker system is a preferred model for studying plasticity in the somatosensory cortex (barrel cortex). Contrarily, only a small amount of research has been conducted to characterize the stability of neuronal population activity in the barrel cortex. We used the mouse whisker system to address the neuronal basis of stable perception in the somatosensory cortex. Cortical representation of periodic whisker deflections was studied in populations of neurons in supragranular layers over extended time periods (up to 3 months) with long-term two-photon Ca^{2+} imaging in anesthetized mice. We found that in most of the neurons (87%), Ca^{2+} responses increased sublinearly with increasing number of contralateral whisker deflections. The imaged population of neurons was activated in a stereotypic way over days and for different deflection rates (pulse frequencies). Thus, pulse frequencies are coded by response strength rather than by distinct neuronal sub-populations. A small population of highly responsive neurons (~3%) was sufficient to decode the whisker stimulus. This conserved functional map, led by a small set of highly responsive neurons, might form the foundation of stable sensory percepts.

Introduction

The somatotopic mapping of individual whiskers to specific areas of the somatosensory cortex is one of the reasons why the whisker system is widely used to study cortical plasticity. For example, whiskers have been cut or removed to study map reorganization (Diamond et al., 1994; Feldman, 2005; Margolis et al., 2012). On the other hand, to date, only a small amount of research has been conducted to characterize the persistency of cortical stimulus representations at the single-cell level (Lütcke et al., 2013) (however, see Masino and Frostig 1996 and Minderer et al., 2011 for studies measuring wide-field signals, and McMahon et al., 2014 for extracellular recordings from individual neurons over months in non-human primates). Plasticity enables us to learn new experiences and adapt to new stimulus conditions, whereas stability of stimulus representation enables us to recognize familiar stimuli even under changing conditions.

Rodents are nocturnal animals and rely on a highly sensitive whisker system. This tactile sense is essential for navigation and object recognition. Rodents are able to actively (whisking) and passively use their whiskers to solve different kinds of tasks, such as roughness discrimination, gap crossing, pole detection, and frequency discrimination tasks (Adibi et al., 2012; Carvell and Simons, 1990; Gerdjikov et al., 2010; Hutson and Masterton, 1986; Jenkinson and Glickstein, 2000; Knutsen, 2006; Mayrhofer et al., 2013; Mehta et al., 2007; Morita et al., 2011). In the somatosensory cortex (S1), inputs from the contra- and ipsilateral whisker pads converge for the first time in the ascending somatosensory pathway (Shuler et al., 2001; Wiest, 2005).

One way to reliably activate the whisker pathway is by rapid changes of the whisker's position (stick-slip events) which correspond to high velocity deflections (Jadhav et al., 2009; Lottem and Azouz, 2009; Wolfe et al., 2008). The frequency of successive stick-slip events – created either by active whisking against a rough surface or by passive deflection when the animal runs along a wall – characterizes the texture of a surface (Arabzadeh et al., 2005). Key questions are how different event frequencies are processed in the barrel cortex and whether simultaneous bilateral activation alters these processes. Whiskers could act as resonators, with each whisker having a distinct characteristic frequency (100–700 Hz). The spatial organization of the whiskers on the rodent's snout would directly translate to frequency representation (Andermann et al., 2004; Moore, 2004). On the other hand, barrel cortex neurons show stimulus locking up to frequencies as high as 1000 Hz (Ewert et al., 2008). This means that a temporal code could be used for differentiating different

* Corresponding author at: Brain Mind Institute, École Polytechnique Fédérale de Lausanne, CH-1015 Lausanne, Switzerland.
E-mail address: johannes.m.mayrhofer@gmail.com (J.M. Mayrhofer).

http://dx.doi.org/10.1016/j.neuroimage.2015.04.045
1053-8119/

frequencies. Alternatively, integrated spike counts have been proposed as a way for the animal to discriminate frequencies (Musall et al., 2014; Stüttgen and Schwarz, 2010).

The present study investigates three main questions: 1) how are different whisker deflection frequencies (pulse frequencies) represented by populations of neurons in the barrel cortex (single barrel); 2) how stable is whisker stimulus representation over time in terms of neuronal population responses; and 3) how stable is the classification accuracy of these stimuli over extended time periods?

Materials and methods

Animals

In total, seven female adult mice (strain: C57BL6J; weight: 20–26 g; Harlan Laboratories, Netherlands) were imaged. The age of the animals on the day of head post implantation was > 14 weeks. Mice were housed individually, with food ad libitum and under an inverted 12-hour light/dark regime. All surgical and experimental procedures were approved by the local veterinary authorities, conforming to the guidelines of the Swiss Animal Protection Law, Veterinary Office, Canton Zurich (Act of Animal Protection 16 December 2005 and Animal Protection Ordinance 23 April 2008).

Head post implantation, virus injection, and cranial window implantation

The animals were anesthetized with isoflurane (1–3%; Abbott, USA). The depth of anesthesia was checked on the basis of hindpaw withdrawal and corneal reflexes. The animal's temperature was maintained at 37 °C by a feedback-controlled heating pad in combination with a rectal temperature probe (Harvard Apparatus, USA). To protect the eyes from desiccation, an ointment was applied (vitamin A eye cream; Bausch & Lomb, Switzerland). Preparation of the animals was divided into two separate surgeries (1–3 weeks apart). In the first surgery, a stereotaxic apparatus was used to fix the animal. Once the skull was cleaned, it was moistened with a water-based gel (Skintact Ultrasonic Gel; Leonhard Lang GmbH, Austria) and a window was positioned at the estimated region of the barrel cortex (1 mm caudal and 3 mm lateral from Bregma) to perform intrinsic optical imaging (IOI; Fig. 1B) with a 630-nm illumination (Margolis et al., 2012). After functionally identifying the barrel cortex, a bonding agent (Gluma Comfort Bond; Heraeus Kulzer, Germany) was applied to the cleaned skull and polymerized (blue light, 600 mW/cm^2; Demetron LC, Switzerland). In order to sculpt the headcap, several layers of transparent light-curing dental cement (Tetric EvoFlow; Ivoclar Vivadent AG, Liechtenstein) were placed on top of the bonding layer. The area of the left barrel cortex was spared for the ensuing virus injection and window implantation. A custom-made aluminum head post was attached (2 mm caudal to Lambda) with additional dental cement. After washing the wound with saline, an antibiotic ointment was applied (Cicatrex; Janssen-Cilag AG, Switzerland). The open skin was sutured and attached to the implant with acrylic glue (Histoacryl; B. Braun, Germany). In the second surgery, a craniotomy above the left barrel cortex was performed (approx. 4 × 4 mm). Virus was injected through thin glass pipettes (Cetin et al., 2007) to the principal whisker area identified by IOI. 150 nl of rAAV hybrid serotype 2/1 (40 nl/min) carrying the Yellow Cameleon 3.60 (YC3.60, under human synapsin promoter) construct was injected at 300-μm depth below the dura mater. To facilitate infection efficiency and spread (Mastakov, 2001) we coinjected a hypertonic D-mannitol solution (1:2, Mannitol 20%; B. Braun, Switzerland). The human synapsin promoter was used to selectively express YC3.60 in neurons (Lütcke, 2010). A square cover slip (3 × 3 mm; UQG Optics Ltd, UK) was lightly pressed on the exposed brain and fixed with dental cement to the headcap. Following the surgeries, the animals were kept warm and provided with analgesics (Novaminsulfon, 50%; Sintetica, Switzerland). During the first week of recovery, an antibiotic was added to the drinking water (Baytril (enrofloxacin), 200 mg/l drinking water; Bayer, Germany).

Whisker stimulation

A single whisker was plugged into a glass capillary (GB 120-8P; Science Products GmbH, Germany; tip was melted to reduce dead space), which was mounted on a piezo actuator (T223-H4CL-303X; Piezo Systems, USA). The control voltage driving the piezo actuator was generated by a custom-written LabVIEW program (National Instruments, USA) using a multifunctional data acquisition card (PCI-6229; National Instruments) and was amplified by a piezo controller (MDT693A; Thorlabs, USA). The amplitude of the stimulator was calibrated using a laser displacement sensor (ILD1700-2; Micro-Epsilon, Germany) (see also Mayrhofer et al., 2013, for an example of recording of stimulus).

The stimulus consisted of a series of deflections to a single whisker (identical whisker for the entire recording period) on the animal's right whisker pads. The deflection was in the anterior–posterior (rostral–caudal) direction. Whiskers were slightly cut to ensure reliable and reproducible single whisker stimulation over days. Depending on the IOI map and the virus expression area, different principal whiskers were used in different animals. The peak velocity of a prototype pulse (taken from a single period 120-Hz cosine wave; peak-to-peak amplitude was 120 μm) was kept constant and the repetition rate of pulses was varied (10, 40, 90, and 110 Hz) on the contralateral side with respect to the imaging side. The stimulus duration was 1 s. The stimulator was placed 4 mm away from the whisker pad and led to a peak-to-peak amplitude of 1.72° and maximum velocity of 648°/s. The stimulus sets were presented in a randomized order within an imaging day to minimize the influence of changes in anesthesia (inter-stimulus intervals: 10–14 s). Each stimulus was presented at least 30 times per imaging day.

Two-photon imaging settings

A 20× water immersion microscope objective was used (W Plan-Apochromat 20×/1.0 DIC VIS-IR; Zeiss, Germany). The genetically encoded Ca^{2+} indicator YC3.60 was excited with a Ti:sapphire laser (870 nm, 140-fs pulses at 80 MHz, Chameleon Ultra II; Coherent, USA). Emission of YC3.60 was detected with two GaAsP photomultiplier modules (H10770PA-40; Hamamatsu Photonics, Japan) with the following filter settings: dichroic mirror 515 DCXR, band pass filter BrightLine HC 542/50 (yellow channel), band pass filter BrightLine HC 475/64 (cyan channel) (Semrock, USA), and short pass filters BrightLine 750/sp for each channel. The two-photon laser-scanning microscope was controlled by custom-written LabVIEW software (National Instruments) (Langer et al., 2013) or ScanImage (Pologruto et al., 2003) running on personal computers using multifunctional data acquisition cards (National Instruments).

Chronic two-photon imaging

Chronic imaging started at the earliest at three weeks after virus injection using a custom-built two-photon laser-scanning microscope (see two-photon imaging settings). Functional signals (128 × 128 and 256 × 128 pixels) were acquired at a frequency of 8-Hz and 11.84-Hz bidirectional scan, respectively. Anatomical imaging was performed with a resolution of 256 × 256 or 512 × 512 pixels. Recordings were performed under isoflurane anesthesia (0.7–1.1%; Abbott). The respiratory rate was monitored with a piezo element (7BB-35-3; Murata Manufacturing Co., Ltd., Japan) attached to an oscilloscope and was maintained at around 150 bpm by adjusting the anesthesia level. A correlation analysis of spontaneous activity (0 Hz, Ca^{2+} response probability) of one session with the previous session (Margolis et al., 2012) showed that Ca^{2+} response probability ($\rho = 0.345$ $p < 0.001$) was significantly correlated. Hence, spontaneous activity was similar over

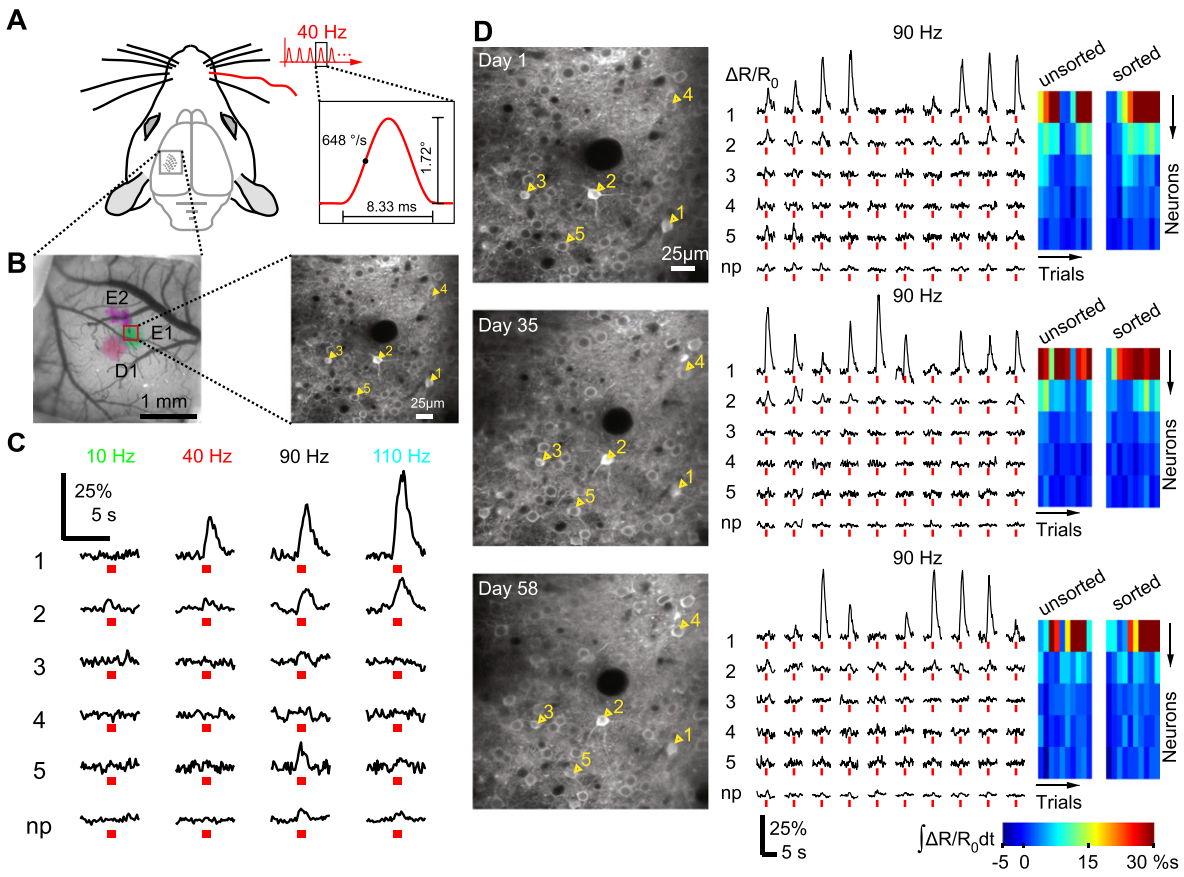

Fig. 1. Stimulation and long-term two-photon Ca^{2+} imaging. (A) Stimulation paradigm: contralateral stimulation relative to the imaging location with pulsatile stimulus (see inset). (B) Chronic window with IOI map of whisker E1, E2, and D1 thresholded and colored overlaid at day 19 after window implantation (left subpanel). Yellow Cameleon 3.60 expression of the red square marked on the left subpanel (right subpanel). (C) Examples of Ca^{2+} transients in response to 10-, 40-, 90-, and 110-Hz 1-s long contralateral pulsatile stimulus (neurons marked in (B) right subpanel and neuropil (np)). Stimulus duration is indicated as red bar below the traces. (D) The same imaging location at different experimental days with 10 Ca^{2+} transient examples from the five marked neurons and the neuropil evoked by a 1-s long 90-Hz stimulus. Stimulus duration is indicated as red bar below the traces. Next to the raw traces, the neuronal response measured as the area under the curve from 0 ms until 2000 ms after stimulus onset ($\int \Delta R/R_0 dt$) is shown color-coded for individual trials and ROIs (left, same order as Ca^{2+} transients; right, sorted according to increasing mean activity of all five neurons).

different sessions, suggesting comparable physiological states of the animal over sessions. For each animal, 1–4 imaging locations (mean ± SD: 2.9 ± 1.1, n = 7 mice) were followed over a time course of up to 3 months (Fig. 2). The average field of view (FOV) was 318 ± 86 µm (mean ± SD, n = 20 FOVs in 7 mice). The medial–lateral and anterior-caudal positions of the imaging locations were chosen on the basis of the IOI mapping and the Ca^{2+} responses. Imaging locations were in the supragranular layers (measured from cortex surface, mean ± SD: 146 ± 62 µm, 20 FOVs in 7 mice).

Data analysis

Data analysis was performed using Matlab (MathWorks, USA) and ImageJ (ImageJ, U. S. National Institutes of Health, USA, http://imagej.nih.gov/ij/, 1997–2012). For each channel, a background subtraction was performed — the minimum pixel value in each imaging movie was found and then subtracted from all pixels of the movie. Regions of interest (ROIs), covering either single neuronal cell bodies or neuropil areas, were drawn manually in ImageJ. Pixel values within each ROI were summed for the yellow fluorescent protein (YFP) and cyan fluorescent protein (CFP) photomultiplier channels separately. Dividing the YFP by the CFP photomultiplier channel value for each ROI generated the ratio time series (R). The mean R value in the 1000-ms pre-stimulus time interval was used as the baseline activity (R_0). Individual ROI ratio changes were obtained by applying the following formula: $\Delta R / R_0 = (R - R_0) / R_0$. ROIs were drawn manually for each imaging day and were matched manually over different experiments in ImageJ. Movies were aligned over trials by maximizing correlations through xy-rigid shifts of the frames. To compare the activity over different stimulus conditions and recordings for each neuron, the $\Delta R/R_0$ from 0 ms to 2000 ms relative to stimulus onset was integrated for each trial ($\int \Delta R / R_0 dt$: area under Ca^{2+} transient in %s) (Helmchen et al., 1996). Spontaneous activity was measured either by using a void stimulus (0 Hz) or by

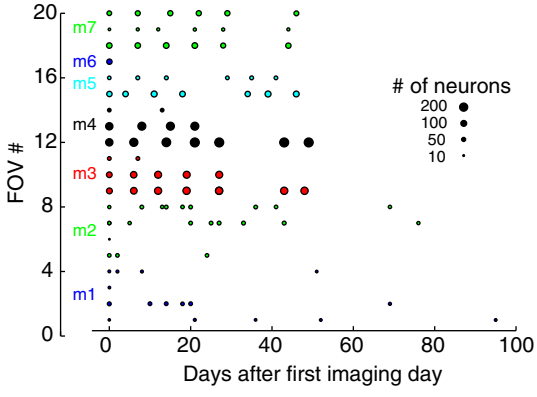

Fig. 2. Overview of all imaged FOVs. Areas of the circles correspond to number of neurons imaged on the corresponding imaging day. Number of individual animals is shown on the left.

shifting the analysis windows back. From these values, a 'population activity vector' for each trial was built where each element corresponded to the stimulus-evoked activity of a single neuron. All population activity vectors of a single imaging day led to the two-dimensional 'population activity matrix' (with neuron identity and trial identity as dimensions). The center of mass activity in a given FOV was computed by taking a weighted average of the x-positions and y-positions of the regions of interest in a FOV:

$$x_{cm} = \sum_{i=1}^{NROI}\left[\int \frac{\Delta R}{R_0}dt\right]_i x_i \Big/ \sum_{i=1}^{NROI}\left[\int \frac{\Delta R}{R_0}dt\right]_i$$

$$y_{cm} = \sum_{i=1}^{NROI}\left[\int \frac{\Delta R}{R_0}dt\right]_i y_i \Big/ \sum_{i=1}^{NROI}\left[\int \frac{\Delta R}{R_0}dt\right]_i$$

where $[\int \Delta R/R_0 dt]_i$ is the integrated activity response of the i-th neuron (see above). NROI is the number of neurons in the consider FOV; x_i and y_i are the center positions of the i-th neuron. The Ca^{2+} response probability of a neuron was obtained by using the Schmitt trigger approach — the Ca^{2+} transient had to cross an upper threshold of 1.75 SD relative to baseline and had to remain above a lower threshold of 0.5 SD for at least another 420 ms (Lütcke, 2010) to be counted as a detected response. The Ca^{2+} response probability was then computed by comparing the number of detected responses to the total number of presented trials. Silent cells were defined as cells which did not show a significantly different Ca^{2+} response probability from spontaneous activity in any stimulus condition (binominal test with Bonferroni correction). Individual pulse frequency response curves were generated by averaging all trials from all recordings of a neuron. Pooling over animals was done by normalizing the responses to the median neuronal activity elicited by contralateral stimulation of each animal (median Ca^{2+} responses: 1.361%s; 1.582%s; 1.343%s; 1.679%s; 0.647%s; 0.713%s; 0.624%s). Correlations between trials of the same or a different stimulus were computed by using the corresponding population activity vector (Pearson's correlation coefficient, corrcoef, Matlab; for a simple population activity vector example see Fig. 1). Reliability–stability matrix: correlation coefficients of the same stimulus and recording day were used to build the reliability values, where correlation coefficients of the same stimulus category but different recording day led to the stability values. The similarity matrix was derived by taking the correlation coefficients between different stimuli within the same recording day. Activity pattern stability was tested by shuffling the population activity matrix either along the neuron identity axis or along the trial identity axis. The neuron-to-neuron correlation was computed by correlating the Ca^{2+} responses of one neuron with the Ca^{2+} responses of a different neuron (~correlation between rows of population activity matrix).

Classification algorithm

For quantification of the discriminability of the different stimuli within an imaging day or over days, a linear support vector machine (Chang and Lin, 2011) was used on the basis of the population activity matrix. This allowed us to decode from the neuronal responses the stimulus identity (5-class classification), i.e. predict the applied pulsed frequency. The discriminability of the stimuli was expressed as the cross-validation accuracy (accuracy) either by training the classifier on one half of the data set and testing it on the other half (2-fold cross-validation, was repeated 10 times, random splitting) or by training the classifier on a data set from one day and testing it with a data set from a different imaging day. To investigate the influence of population size on the representation of the stimuli, a neuronal population was generated from all recordings (FOVs, days, and animals) — from each day, only 50% of the trials with highest activity were considered. From this remaining data set, only neurons for which more than 100 trials were available entered the data set and 100 trials were chosen randomly. Population size was varied either by randomly picking neurons from the data set, by choosing neurons starting with highest activity or by choosing neurons starting with lowest activity. In the case of random selection of neurons, the selection was repeated six times (total number of neurons in data set) / (current number of neurons considered) for the computation of the similarity and discriminability. The accuracy for each chosen population was derived by the 2-fold cross-validation of 10 times.

Statistics

Statistical errors are standard errors of the mean (SEM) unless otherwise specified. The Wilcoxon signed rank test or paired Student's *t*-test and Kolmogorov–Smirnov test (Matlab implementation) were used to statistically test differences between two dependent groups and independent groups. One-way ANOVA combined with Tukey post-hoc test was used to statistically assess the differences between groups (Matlab implementation). Correlations were computed using Pearson's correlation coefficient (Matlab implementation).

Results

Chronic two-photon Ca^{2+} imaging and stimulation paradigm

To follow the activity of the same population of neurons over long periods of time, chronic two-photon Ca^{2+} imaging of a genetically encoded Ca^{2+} indicator (GECI; YC3.60) was performed in the barrel cortex of anesthetized mice (n = 7 animals; see Materials and methods). Pulsatile stimulus trains (1-s duration) with different repetition rates of 10, 40, 90, and 110 Hz were used to stimulate a single contralateral vibrissa (vibrissa identity was kept constant over experimental days; Fig. 1A). IOI was performed to visualize the barrel representation (Fig. 1B, left subpanel) which was used for identification of the GECI injection site and the respective imaging FOV during two-photon imaging (Fig. 1B, right subpanel). The typical YC3.60 expression spares out the nucleus and only labels the neurons' cytosol. The soma appears as a ring or filled circle depending on the z-position of the imaging plan with respect to imaged neuron. The area under the Ca^{2+} transient represented the stimulus-evoked activity of a single neuron ('Ca^{2+} response') for the different frequencies of periodic whisker deflections (Fig. 1C, see Materials and methods). For moderate firing frequencies (i.e. no saturation effects: <15 Hz; ~7 action potentials (APs)), the area under the Ca^{2+} transient is proportional to the total number of APs (Lütcke, 2010). The combination of the chronic window preparation and ratiometric GECI allowed repeated functional monitoring of populations of neurons over time periods as long as 3 months (Fig. 2). Since the Ca^{2+} signal is ratiometric (see Materials and methods), it is less dependent on the expression level over time compared to single-fluorophore GECIs. On average, neurons were followed over a time span of 35 ± 19 days (mean ± SD, n = 1548 neurons in 7 mice), where an entire imaging location (i.e. FOV) was functionally monitored for 39 ± 27 days (mean ± SD, n = 20 FOVs in 7 mice). The average number of neurons per FOV and day was 71 ± 58 (mean ± SD, n = 20 FOVs in 7 mice) (Fig. 2). Fig. 1D shows a typical area at different experimental days with responses to a 90-Hz stimulus. In addition, the population activity matrix for the chosen neurons is illustrated. It was built by reporting the integrated Ca^{2+} response in every trial (columns) and for each neuron (rows).

Ca^{2+} responses in barrel cortex neurons increase in a sublinear manner with an increasing number of whisker deflections per second

We first characterized the spontaneous (0 Hz) and stimulus-evoked (10, 40, 90, and 110 Hz) activity of single neurons. Since barrel cortex neurons display adaptation to periodic whisker deflections (Khatri, 2004; Melzer et al., 2006), the Ca^{2+} response was plotted against stimulus pulse frequency with a logarithmic x-scale. Fig. 3A shows the Ca^{2+}

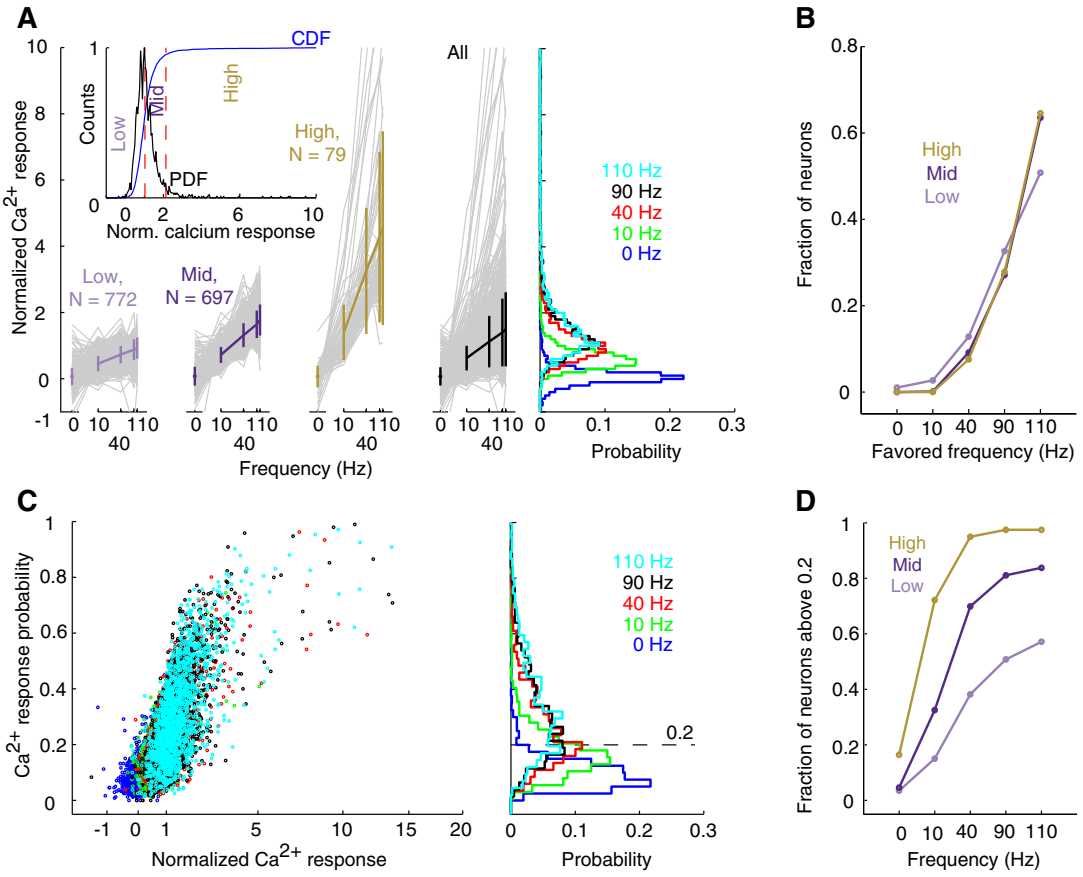

Fig. 3. Whisker deflection frequency representation: individual neuronal Ca^{2+} responses. (A) Average neuronal Ca^{2+} responses of all recorded neurons (category 'All', n = 1548 neurons in 7 mice) and for different response categories ('Low', 'Mid', and 'High'). The inset shows the histogram of the mean response amplitude of all contralaterally presented stimuli of the individual neurons (PDF: probability density function; CDF: cumulative density function). This distribution was used to classify the neurons as follows: 'Low' (0–50%), 'Mid' (50–95%), and 'High' (95–100%) responders. Gray traces show averaged pulse frequency response curves of individual neurons. The average and SD is shown in black. On the right, the histogram of the response amplitude for the different stimulus categories is presented. (B) Plot of how many neurons displayed their peak response at 0, 10, 40, 90 or 110 Hz (favored pulse frequency) for the response categories shown in (A). (C) The average Ca^{2+} response probability is plotted over the average response amplitude for different stimulus categories for all neurons (n = 1548 neurons in 7 mice, x-axis in log scale). Each dot corresponds to an individual neuron. On the right, the histogram of the Ca^{2+} response probability for the different stimulus categories is shown. (D) Plot of how many neurons were on average activated at least in each fifth trial over the different whisker deflection frequencies for the response categories shown in (A).

response to the different frequencies of whisker deflections of all neurons and animals. Since the average Ca^{2+} response of the recorded neurons was broadly distributed (Fig. 3A, right subpanel), neurons were divided into three categories (high, medium, and low responding neurons, see inset of Fig. 3A). Data were pooled for all animals after normalizing the responses of each animal to its median Ca^{2+} response over all whisker stimuli and recorded neurons. The average neuronal activity of individual neurons as well as the entire population activity increased in a sublinear (log) manner with an increasing number of whisker deflections per second (2-fold increase for 10-fold higher stimulus pulse frequency). A total of 886 out of 1548 neurons increased their Ca^{2+} responses with the pulse frequency; 1349 (87%) out of 1548 neurons showed their highest Ca^{2+} response at either 90 Hz or 110 Hz (Fig. 3B). No clear difference of the distribution of favored pulse frequency over different response categories was seen (Fig. 3B). To determine whether the neurons which showed on average a high stimulus-evoked response are also the ones which responded most reliably over the trials, the 'Ca^{2+} response probability' was computed. The Ca^{2+} response probability quantifies how often a neuron is activated above a baseline-derived threshold in response to the stimulus (see Materials and methods). Neurons with a high average response were more often activated (n = 1548 neurons in 7 mice, correlation for 0 Hz: $\rho = 0.493$, 10 Hz: $\rho = 0.484$, 40 Hz: $\rho = 0.613$, 90 Hz: $\rho = 0.608$, and 110 Hz: $\rho = 0.597$; Fig. 3C). Additionally, higher whisker deflection frequencies more often evoked a detectable Ca^{2+} transient as compared to low pulse frequencies (Fig. 3C). At a whisker stimulus above 40 Hz, the population size of repeatedly activated neurons (neurons with a Ca^{2+} response probability above 0.2) remained almost unchanged (Fig. 3D). The correlation between Ca^{2+} response probability of spontaneous and stimulus evoked response probability was found to be significant in all categories (Bonferroni corrected $\alpha = 0.0125$; $\rho = 0.515$ for 10 Hz, $\rho = 0.429$ for 40 Hz, $\rho = 0.329$ for 90 Hz, $\rho = 0.275$ for 110 Hz; $p < 0.001$) consistent with Fig. 3D. The number of silent cells was 29.9% of the total population. Silent cells were defined as cells which did not show a significantly different Ca^{2+} response probability from spontaneous activity in any stimulus condition (binominal test with Bonferroni correction). The spatial distribution of activity within imaging FOVs (imaging locations were centered on the barrel) was similar in shape for the higher pulse frequencies, with an increased Ca^{2+} response in the center of the barrel column (Fig. 4A). At barrel borders, pulse frequency selectivity was lower compared to the barrel center, caused by a decreased Ca^{2+} response difference for the different whisker stimuli. The average Ca^{2+} response was in general lower for neurons located more superficially, putatively interneurons (Lefort et al., 2009) (Fig. 4B). We also found an increased neuron-to-neuron correlation with increased stimulus strength; neurons closer to each other showed an increased stimulus-induced correlation (Figs. 4C and D) (Kerr et al., 2007). The 12 most active neurons showed an average distance of 72 ± 32 μm (radius; mean ± SD; median was 68 μm) from the barrel center. These high responding neurons are located in the barrel column

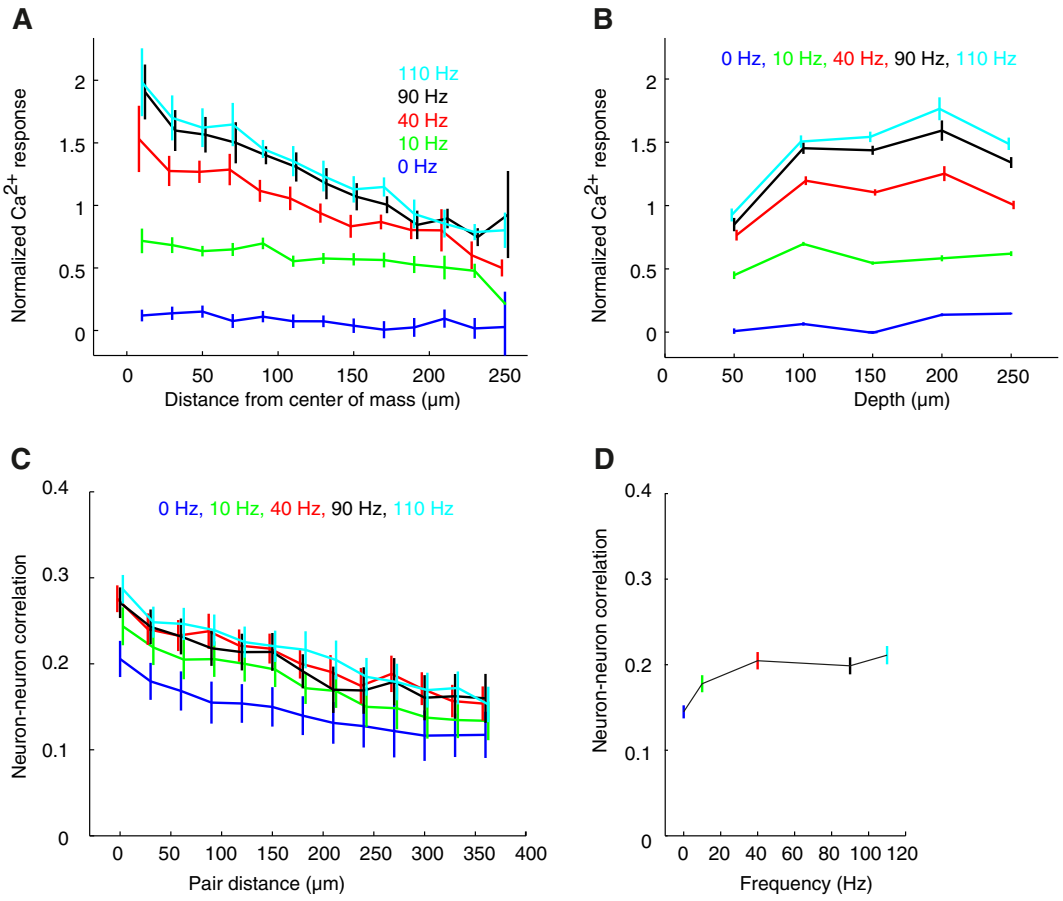

Fig. 4. Spatial distribution and neuron-to-neuron correlation of Ca^{2+} responses. (A) Spatial distribution of Ca^{2+} responses. The average Ca^{2+} response over distance measured from the center of mass of activity in a given FOV is plotted. The center of mass for activity was computed for each session individually (SD of center of mass for activity over sessions for X = 8.5 ± 1.4 μm and Y = 9.5 ± 1.3 μm, n = 17 FOVs in 6 mice). (B) Depth dependency of Ca^{2+} responses (mean ± SD). (C) Neuron-to-neuron correlation is plotted over the pair distance (n = 20 FOVs in 7 mice). Stimulus-evoked Ca^{2+} responses of neurons in the same FOV were correlated with each other. Neurons which are further apart show a smaller correlation than close by neurons. With increased stimulation strength a stronger pairwise correlation is seen (D). Plots and values are mean ± SEM. Statistical analysis: Kolmogorov–Smirnov test.

(~150 μm in radius; (Lefort et al., 2009)) but are well distributed therein (SD = 32 μm).

Different whisker deflection frequencies elicit similar ensemble activity patterns

How are different event frequencies (cf. stick-slip event rates) represented by the population of neurons in the somatosensory cortex? To characterize whether different pulse frequencies activate different activity patterns in the barrel cortex, the correlation coefficient of the activity vectors between different whisker deflection frequencies was calculated (for each trial, but only within one day) (Niessing and Friedrich, 2010). A high correlation between different stimuli indicates that the stimulus-induced activity patterns are similar. Low correlation can be caused either by little stimulus-driven activity or by different activation patterns evoked by different stimuli. The latter case would result in a high correlation for one particular stimulus (high reliability) but a low correlation between different stimuli (low similarity). Fig. 5A shows an example population activity matrix for different stimuli from one FOV and Fig. 5B illustrates the corresponding similarity matrix. The upper/right triangular part shows the single trial-to-trial correlation coefficients for the different stimuli (self-correlation was omitted). The lower/left triangular part displays the mean correlation for the different stimulus comparisons. Pooled over FOVs (20 FOVs in 7 mice), the similarity matrix attained the form shown in Fig. 5C. For the 10-Hz stimulus, a weak correlation with the other whisker deflection frequencies was seen. This is due to the fact that the 10-Hz stimulation evoked only weak pattern activation (small reliability value; Fig. 3). For higher whisker deflection frequencies, the correlation increased between stimuli and for the individual stimulus (higher reliability). The right subpanel of Fig. 5C compares neighboring pairs of matrix elements. The similarity of the pairs shows that different whisker deflection frequencies elicited similar activity patterns, indicating that different pulse frequencies did not activate distinct populations of neurons — most strongly seen for 90- and 110-Hz stimulation. This agrees with the observation that more neurons were not measurably activated but the evoked Ca^{2+} response increased with pulse frequency (Fig. 3D).

High whisker deflection frequencies are reliably and stably represented in the neuronal population

How stable is the representation of a certain whisker stimulation (e.g. 90 Hz) in the barrel cortex over different timescales (minutes to days)? The reliability–stability matrix was derived by correlating the population activity vectors from different trials either from the same imaging day (reliability) or from different days (stability) with each other (Bathellier et al., 2012). Fig. 6B shows the matrix for the population activity matrix example in Fig. 6A. The upper/right triangular part of the matrix shows the single trial-to-trial correlations (self-correlation was removed). The mean single trial-to-trial correlation within imaging

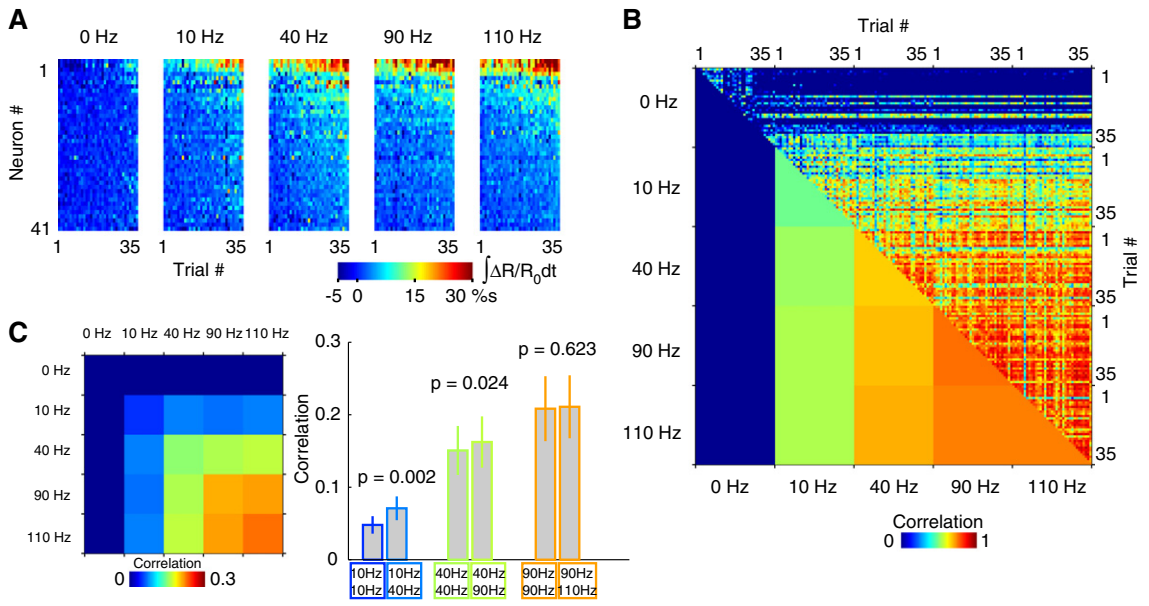

Fig. 5. Whisker deflection frequency representation: population responses of S1 ensembles. (A) Example population activity matrix for 0 (spontaneous activity), 10, 40, 90, and 110 Hz (35 trials per stimulus category). (B) Similarity matrix of the same neuronal population as shown in (A). The upper triangular part of the matrix shows the individual trial-to-trial correlation of the population activity for one stimulus and for two different stimuli in a single day (self-correlation was omitted). The lower part shows the averages of the trial-to-trial correlations for one stimulus and for two different stimuli in a single day. The diagonal elements correspond to the average reliability of a stimulus (see Fig. 6). (C) Similarity matrix for all FOVs (n = 20 FOVs in 7 mice). Right subpanel: comparison of several matrix elements with each other, e.g. '10 Hz 10 Hz' (reliability for 10 Hz) vs. '10 Hz 40 Hz' (similarity between 10 Hz and 40 Hz). Plots are mean ± SEM. Statistical analysis: Student's *t*-test.

day is shown in the lower/left part. Another way of presenting the averaged matrix elements is to plot them over their inter-session intervals (time spans between imaging days; Fig. 6C). For this example, there was no correlation of the reliability–stability matrix elements with the inter-session interval, indicating that the trial-to-trial variability within a day was in the same range as over different days (n = 15 matrix elements, $\rho = -0.096$, $p = 0.732$). In Fig. 6D, the diagonal elements (mean intra-day correlation: reliability; n = 5 matrix elements) and off-diagonal elements (mean inter-day correlation: stability; gray shaded; n = 10 matrix elements) are shown as mean values. To elucidate whether there is a certain stereotypical activity pattern in the population, the matrix elements were compared to the case where the activity vectors were shuffled along the neuron ID axis within a trial. Both the reliability and stability dropped to near-zero values. Shuffling the activity matrices along the trial ID axis for each neuron individually did not change the correlation significantly, demonstrating the existence of a stereotypical activity pattern which remained constant over trials and days.

Fig. 6E displays the matrix elements of pooled imaging areas plotted over the different whisker deflection frequencies: bar plots for reliability (intra-day correlation, n = 20 FOVs in 7 mice), stability (inter-day correlation, gray shaded, n = 17 FOVs in 6 mice), and shuffled along neuron ID and trial ID axis cases for the reliability case. The highest correlation values were achieved for the high pulse frequencies. On average, the reliability (mean trial-to-trial correlation within a day) was not significantly higher than the stability (mean trial-to-trial correlation over days) and remained for both well above the control condition in which the neuron ID was shuffled (Fig. 6E, red bars vs. blue bars). Shuffling along the trial ID axis reduced the reliability, but not to the level of the stability matrix elements (Fig. 6E, green bars). Hence, there was a stereotypic activation of the imaged neuronal ensemble that was preserved over days compared to activation of the population at random. Furthermore, increased stimulus strength in terms of higher pulse frequency established a more reliable and stable network activation (n = 20 FOVs in 7 mice, correlation between reliability and whisker deflection frequency: $\rho = 0.510$, $p < 0.01$; n = 17 FOVs in 6 mice, correlation between stability and stimulus strength: $\rho = 0.494$, $p < 0.01$; see also Fig. 6C). A non-significant correlation of the reliability–stability matrix elements with the inter-session interval was seen, indicating that the trial-to-trial variability within a day was in the same range as over different days (n = 352 matrix elements in 7 mice: 0 Hz: $\rho = -0.016$, $p = 0.763$; 10 Hz: $\rho = 0.029$, $p = 0.593$; 40 Hz: $\rho = -0.032$, $p = 0.546$; 90 Hz: $\rho = -0.048$, $p = 0.370$; 110 Hz: $\rho = -0.054$, $p = 0.316$; see Fig. 6D as example).

Stable classification accuracy over extended time periods

We have previously investigated the ability of rodents to discriminate different frequencies of bilateral whisker deflections. In general, rats and mice trained in the identical task showed similar psychometric curves and behavioral readouts (Mayrhofer et al., 2013). However, it remains unknown how such stimuli are represented in the population activity of cortical neurons over an extended period of time. To this end, we applied a machine learning approach (linear support vector machine) in order to identify how well the system can maximally discriminate different whisker stimuli based on the neuronal activity we detected in S1 (see Materials and methods). Ultimately, our objective was to elucidate whether long-term aspects of the neuronal stability or variability are reflected in the classification accuracy. The individual neurons were taken as features for the classification. In Fig. 7B (left subpanel), a single FOV classification result is shown for the activity matrix shown in Fig. 7A. Along the y-axis the ID of the training day is shown, whereas the x-axis corresponds to the sample ID (=ID of 'test' data set). Hence, for example, the first row indicates that the classifier was trained on the first data set from the first day (or subset in the case of intra-day classification, see Materials and methods) and tested (cross-validated) on all other days in the data set (or the subset which was left in the case of intra-day classification). The matrix is summarized in the right subpanel of Fig. 7B. Here, the diagonal elements correspond to the intra-day accuracy (cross-validation within a day) and the off-diagonal elements to the inter-day accuracy (cross-validation over different days) of the classification algorithm. For both cases, a performance

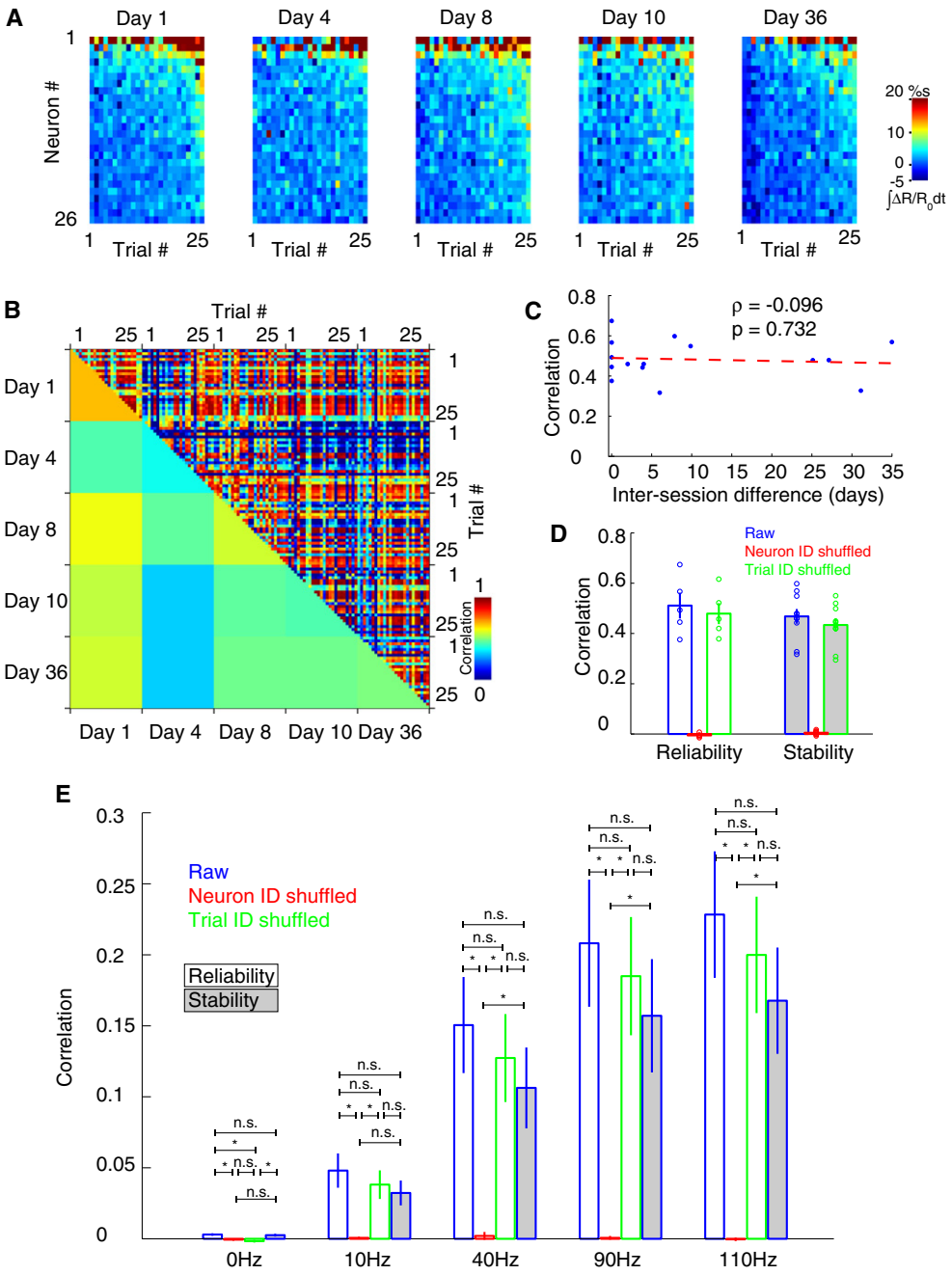

Fig. 6. Reliability and stability of whisker stimulus representation in S1. (A) Example population activity matrix for 90-Hz contralateral stimulation from the same population of neurons over different experimental days (25 trials per day/session). (B) Reliability–stability matrix of the same neuronal population as shown in (A). The upper/right triangular part of the matrix shows the individual trial-to-trial correlation of the population activity within a session (day) or over different days. The lower/left part shows the averages of the trial-to-trial correlations within a day or over two different days. The diagonal corresponds to the reliability of a stimulus representation, whereas the off-diagonal elements represent the stability of the stimulus representation. (C) Average correlation of the reliability–stability matrix over the inter-day difference for 90 Hz for the example shown in (A). (D) Comparison of the stimulus representation reliability with the stability over days (blue). The reliability and the stability are also shown for the same data set where either the neuron ID or the trial ID was shuffled. (E) The reliability and stability values of the stimulus representation for different whisker deflection frequencies (0 Hz: spontaneous activity) are shown for all FOVs ($n = 20$ FOVs in 7 mice). In addition, the reliability where either the neuron or trial ID was shuffled is depicted. Plots are mean ± SEM. Statistical analysis: Pearson's correlation and one-way ANOVA (0 Hz: $F_{3,73} = 6.51$; 10 Hz: $F_{3,73} = 5.31$; 40 Hz: $F_{3,73} = 6.13$; 90 Hz: $F_{3,73} = 6.9$; 110 Hz: $F_{3,73} = 8.64$ all p-values < 0.0023) with Tukey post-hoc test at significance of $p < 0.05$ (*); not significant (n.s.).

above chance (20% for five different stimuli) was reached ($n = 16$ matrix elements, $p < 0.001$). The classifier was able to differentiate the stimuli within a day and over days (Fig. 7B, right subpanel). Pooled over animals and FOVs, the classification accuracy was well above chance, meaning that the stimuli could be discriminated within a day ($n = 20$ FOVs in 7 mice, $p < 0.01$) and over days ($n = 17$ FOVs in 6 mice, $p < 0.01$) with a pre-set decision criteria derived from the same or a different day (Fig. 7C, red bars: 'Population'). Neurons can be used as features for the classifier to discriminate stimuli within a day and over days. This demonstrates a considerable stability of the population activity pattern over days.

In order to address the question of whether the information about the identity of the individual neurons (neurons as classification feature: 'Population') improves discrimination performance, the mean activity

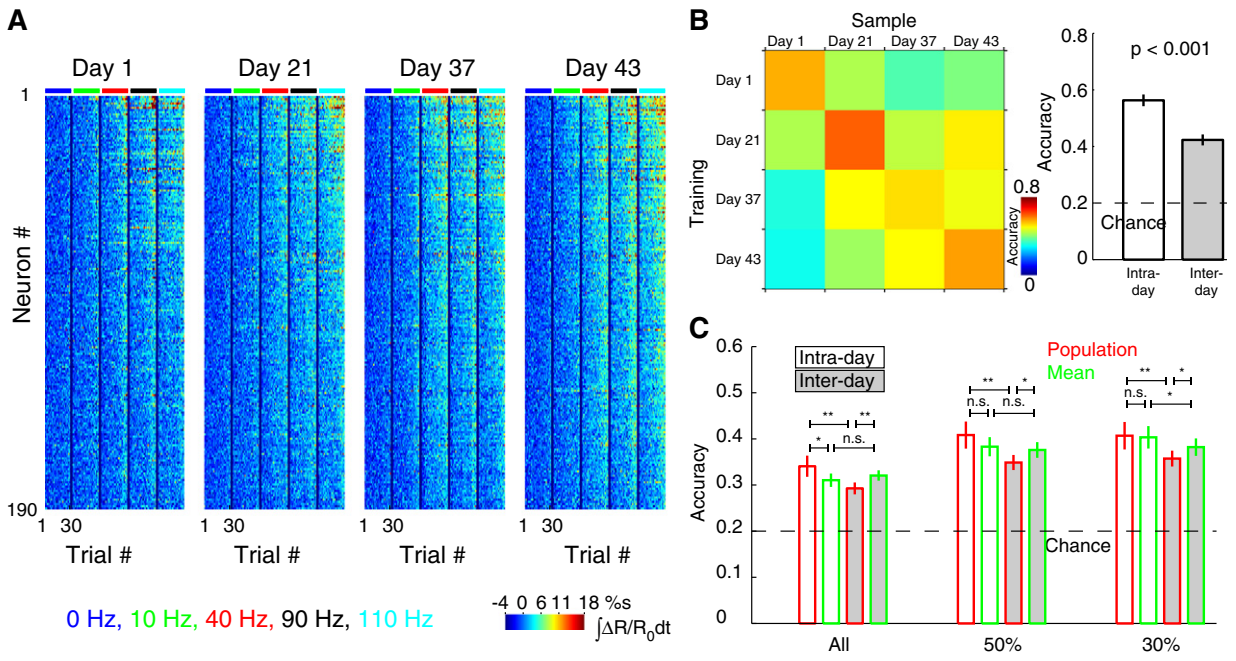

Fig. 7. Classification accuracy of pulse frequencies. (A) Example population activity matrix for 0- (spontaneous activity), 10-, 40-, 90-, and 110-Hz stimulation from the same imaging location over different experimental days. Thirty-one trials per stimulus pulse frequency are presented. Trials were sorted for each stimulus pulse frequency according to the mean response amplitude of the population. Neurons were sorted with respect to their mean response amplitude over all trials, experiments, and stimulus pulse frequency. (B) Left subpanel, discriminability matrix: classification accuracy (cross-validation) over days for the same data set shown in (A). The y-axis indicates which day was used for training the classifier and the x-axis labels show the sample day for cross-validation. Right subpanel shows the mean of the intra-day accuracy (diagonal elements of the discriminability matrix on the left) and the inter-day accuracy (off-diagonal elements of the discriminability matrix on the left). (C) Classification accuracy within days (n = 20 FOVs in 7 mice) and over days (n = 17 FOVs in 6 mice) for different classification criteria for all FOVs. Left ('All') shows the accuracy for all trials of the data sets, middle block ('50%') accuracy for the 50% highest activity trials, and right ('30%') accuracy for the 30% highest activity trials. 'Population' (red bars) corresponds to the case where the neurons were used as classification features, whereas in the case of 'Mean' (green bars) the mean activity of the entire neuronal ensemble of a FOV was used as a classification feature. Plots are mean ± SEM. Statistical analysis: Student's *t*-test. $p < 0.05$ (*), $p < 0.01$ (**), and not significant (n.s.).

of all neurons of the FOVs (i.e. 'Mean') was taken as a classification feature for comparison (Fig. 7C, green bars: 'Mean'). In both cases, all neurons in the corresponding FOV were taken into account. On average, the two classification methods did not perform differently for intra-day discrimination of the stimulus categories for the more active trials (n = 20 FOVs in 7 mice; All, $p = 0.02$; 50%, $p = 0.07$; and 30%, $p = 0.81$), whereas a difference was seen for the classification performance over days. Here, the 'Mean' criterion performed better than the 'Population' criterion (n = 17 FOVs in 6 mice; All, $p < 0.01$; 50%, $p < 0.05$; and 30%, $p = 0.05$). The mean activity is better suited to differentiate whisker stimuli because it is less prone to slight changes in the population activity distribution within the population. When only the 50% or 30% most active trials of a given data set were considered, the results generally were very similar, but the classification accuracy was superior (Fig. 7C; '50%' and '30%'). Therefore, trials with low stimulus-evoked activity diluted the information about the stimulus identity. Taken together, we observed a stable classification accuracy by a stable neuronal population activity for the different whisker stimuli over extended time periods.

Highly active neurons are best at encoding the vibrotactile stimuli

The barrel cortex showed sparse responses to whisker stimulation manifested in the long-tailed response distribution (Fig. 3A; Barth and Poulet, 2012; Petersen and Crochet, 2013). Is there a critical population size of neurons overlapping with highly responsive neurons to reliably represent and decode the stimulus identity? A neuronal population was generated by pooling neurons from all recorded data (Fig. 8A, in total 467 neurons and 100 trials per stimulus from 6 mice, see Materials and methods). What is the contribution of the most active neurons to the reliability and similarity of the stimuli? The population from Fig. 8A was taken and varied in three different ways. One way was to include first the most active neurons, leading to a fast increase of the reliability of a stimulus and decreasing again with an increased population size (Fig. 8B, red line). This can be seen as adding noise to the system. When the least active neurons were taken first, again an increase was observed, but the reliability remained rather low when compared to the random sampling and 'most active first' scenarios. Only when the most active neurons were added, it reached the final value (Fig. 8B, blue line). In the third scenario, where neuronal populations were generated by randomly selecting neurons from the data set (for each population size this selection procedure was repeated multiple times, see Materials and methods), the reliability increased with population size (Fig. 8B, green line). Concerning the similarity between stimuli, a comparable result was seen. Adding first the most active neurons markedly increased the correlation between stimuli (data not shown). Hence, the activity pattern elicited by the different stimuli was governed by a small number of neurons which were the most active ones in the population and the low active neurons added variance to the stimulus representation.

Are these highly responsive neurons also best at decoding the stimulus identity? Different population sizes were generated by randomly selecting neurons from the data set. For each population size, this selection procedure was repeated multiple times (see Materials and methods). For each population size, half of the data set was used to train the classifier and then to test it on the rest of the data set. The classification accuracy increased monotonically with increased population size, already reaching 80% of its top performance for the population size of 117 neurons (Fig. 8C). A fit of the form $y(x) = A - B * \exp(-x / C)$ was performed to extract this value (fit parameters: $A = 0.7003$, $B = 0.3118$, $C = 147.5682$; R^2 of fit 0.97). If the population was ordered in a systematic way by including high responding neurons

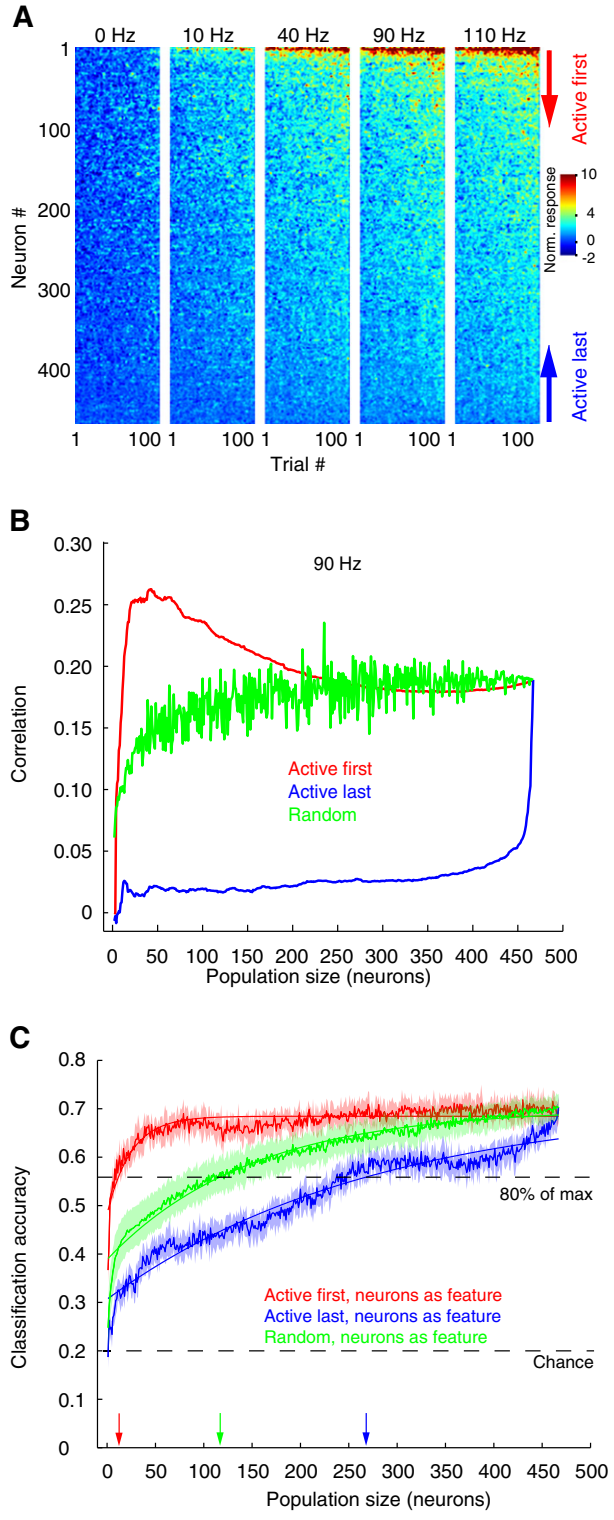

Fig. 8. Critical population size. (A) Population activity matrix for 0- (spontaneous activity), 10-, 40-, 90-, and 110-Hz stimulation derived from all recordings (100 trials per stimulus category). Matrix was smoothed (Gaussian low-pass filter) for illustration. (B) Reliability of 90-Hz stimulus over different population size varied in three different ways: active neurons were added first, least active neurons were added first, and random selection of neurons (see also arrows in (A)). (C) Classification accuracy over different population size was tested in three different ways as in (B). Thin lines correspond to fits of the form: $y(x) = A - B^{*}\exp(-x / C)$. Plots are mean ± SD.

first and least active neurons last, only the 12 most active neurons were required to reach 80% of the classification top performance (A = 0.6845, B = 0.2018, C = 24.7770; R^2 of fit 0.77). Conversely, where the population was generated by including first the least responding neurons and last the highly active neurons, an increase of the classification performance similar to the randomly chosen sample was seen for small population sizes. However, a much larger number of neurons (268 neurons) was needed to reach the 80% level (A = 0.7126, B = 0.4060, C = 275.8131; R^2 of fit 0.95; Fig. 8C).

Discussion

Using chronic two-photon Ca^{2+} imaging in mice, we found a stable and stereotypic representation of whisker stimuli in supragranular layers of the somatosensory cortex that was preserved over months. Stimulus-evoked activity increased for higher pulse frequencies in almost all neurons (87%). In addition, the network activity patterns elicited by the different whisker deflection frequencies were relatively stable over time, reflected in a similar inter- and intra-day variability and a stable classification accuracy. Different pulse frequencies did not activate orthogonal population activity patterns (as defined in (Srivastava et al., 2008)) in the somatosensory cortex, indicative of similar representation of the different whisker deflection frequencies at the network level. A small population of highly responsive neurons (~3%) was sufficient to decode the different whisker stimuli.

Since the amplitude of the measured Ca^{2+} transient is linearly proportional to the neuronal firing (<15 Hz, <7 APs, see Lütcke, 2010), an increased mean Ca^{2+} response can be related to an increased integrated firing (Helmchen et al., 1996). In general, we found increased firing with increased stimulation pulse frequency and almost all neurons showed their highest activity at the highest pulse frequencies (Fig. 3) (Arabzadeh et al., 2003; Melzer et al., 2006). In addition, repetitive whisker deflection leads to adaptation of single neuron responses, i.e. neuronal responses are generally higher for the first whisker deflection compared to subsequent events (frequency-dependent adaptation, see Khatri, 2004; Melzer et al., 2006; Musall et al., 2014), but can still be locked to the stimulus (Ewert et al., 2008). Our results suggest a similar effect from the sublinear increase of Ca^{2+} responses of the neuronal population upon elevated pulse frequency (Fig. 3). At this point, we cannot exclude that for neurons with high Ca^{2+} amplitudes (putatively bursting neurons; Lütcke, 2010) a saturation of the Ca^{2+} indicator is masking non-adaptive neurons. To resolve this possibility, one would need to record action potentials from these neurons.

At the population level, we observed that different pulse frequencies do not activate different populations of neurons. Diverse whisker deflection frequencies elicited similar spatial response patterns in the neuronal populations imaged (Figs. 3D, 5). Modulation of activity can be seen as a fixed subpopulation of neurons which is altered according to the stimulus strength. In our stimulus setting, we varied two independent parameters at the same time: number of pulses (train length) and rate of pulses (pulse frequency). In the case of a clear pulse frequency-dependent spatial representation, one would expect this representation to be independent from the stimulus train length. We conclude that passively received whisker deflections, at least in the applied frequency range, do not seem to be represented in discrete states. At this point, it remains open how pulse frequencies are processed in a single barrel, either by the firing rate and/or the exact timing of neurons. Previous studies show that stimulus history potentially changes the representation of direction selectivity and improves neuronal detection performance for one direction over the other (Li and Ebner, 2007; Tsytsarev et al., 2010). Since our stimulus consisted of a series of deflections in only one direction this could have facilitated our response for high stimulation frequency. Also a change of excitability of GABAergic neurons (depending on the state of the mouse e.g. awake versus anesthetized) could influence the direction selectivity down to the principal trigeminal nucleus (Bellavance et al., 2010). Here, we have neither investigated the direction dependency nor anesthesia effects on frequency coding.

When we looked at the stability of stimulus representation over time, we found a stereotypic activation pattern in the imaged population

of neurons within a day and over weeks (Fig. 6). As soon as the neuron ID was shuffled, the correlation between trials within a day and over different days was lost. This indicates a strong preservation of neuronal activity distribution within local ensembles of neurons and firmly agrees with the finding of Margolis et al. (2012) that sparse activity is stable over weeks. This is also supported by the finding that response probability, latency, stimulus preference, and spontaneous activity can be stable in individual neurons over two weeks (Cohen et al., 2013). Sparse activity manifested in the long-tailed activity distribution (Fig. 3A) has been observed repeatedly in the somatosensory cortex in recent years (Barth and Poulet, 2012). Here, we found that not only the sparse activity is stable over months but its spatial distribution is also preserved. The functional role of this sparse firing in layer 2/3 neurons could be a high stimulus selectivity (Petersen and Crochet, 2013), in our case for repeated single whisker deflection in one direction. It is still unclear how this sparseness is functionally implemented in the cortex. A strong recurrent inhibition could reduce the overall firing output from pyramidal neurons and increase the sparseness of response probabilities (Crochet et al., 2011; Gentet et al., 2010; O'Connor et al., 2010).

We have previously shown that when rodents are trained to discriminate pairs of different pulse frequencies, they demonstrate a rather large variability in their learning phase duration (Mayrhofer et al., 2013). Furthermore, they show stable perceptual interpretation of the presented pulse frequencies by successfully discriminating the different stimuli over weeks. The stimulus-evoked activity of individual neurons can be used as a feature (the spatial activity pattern is taken into account) to discriminate whisker stimuli within a session or over longer time periods. We observed an improved decoding performance of the different stimuli over days by taking the mean activity of the population as the classification feature instead of using the individual neurons as features (Fig. 7C). This superiority of the use of the mean activity to discriminate pulse frequencies over days most likely stems from it being less sensitive to slight changes in the population activity distribution compared to the case where neurons are used as features. Therefore, it would be advantageous for the animal to use the mean population activity for stimulus comparison over days. Stable discriminability of whisker stimuli based on neuronal responses was found to be reflected by the animal's performance during a vibrotactile discrimination task with the same pulsatile stimuli (Mayrhofer et al., 2013).

Our data revealed that a small group of neurons (~3%) showing a large and reliable stimulus-evoked activity is sufficient to discriminate the different stimuli to a large extent. These high responders – which could be excitatory cells (Barth and Poulet, 2012; O'Connor et al., 2010; Yassin et al., 2010) – could be the result of rare large-amplitude synaptic connections which drive these neurons in a reliable way (Lefort et al., 2009). The reliability of this small subpopulation of highly responsive neurons was found to be highest compared to the least active neurons (Fig. 8B). On the other hand, a large fraction of the neurons showed a weak response to stimulation and responded stochastically over trials. However, a large population of these low responding neurons again led to high prediction strength of the stimulus (Fig. 8). Two distinct and complementary coding strategies could be the basis of these observations: 1) A sparse coding strategy occurs in a relatively small subpopulation of neurons, which is activated in a stereotypic way over trials. This sparseness is preserved over long periods (weeks) and could be the neuronal basis for a constant percept. 2) A weak activation and higher response variability occur in individual neurons, resulting in a high prediction of the stimulus by reading out the activity of a large neuronal population. The results of the present study indicate that most information about whisker deflection frequency is carried by a small number of neurons (~3% in the supragranular layers, see Fig. 8) and that this information is sufficient to account for most of the neuronal stimulus classification success (80%). These results clearly favor the first option and support a sparse coding hypothesis (Olshausen and Field, 2004). It has recently been shown that texture encoding is heterogeneous and sparse in the rat barrel cortex (Safaai et al., 2013), supporting our current finding. There is additional experimental evidence that rats use the integrated spike count (which is proportional to the Ca^{2+} response measured here (Lütcke, 2010)) to discriminate frequencies (Gerdjikov et al., 2010; Stüttgen and Schwarz, 2010) or spike rates to differentiate between textures (von Heimendahl et al., 2007). In mice trained to detect a photostimulus (light activation of channelrhodopsin-2 expressed in layer 2/3 neurons), only a small subset of neurons (<1%) was sufficient to drive a reliable behavior (Huber et al., 2008), causally linking the sparse activity in layer 2/3 to perceptual decisions and learning. Similarly, psychophysical thresholds for frequency discrimination in primates are best reflected by the neuronal firing rate (Hernández et al., 2000; Luna et al., 2005; Salinas et al., 2000). Mice trained in surface discrimination and object detection show behavior-dependent recruitment of long-range projection neurons (Chen et al., 2013). It remains open whether these projecting neurons overlap with the sparse population of highly active neurons identified here and act as 'hub' cells to deliver sensory evidence to areas downstream. Since we did not address the identity of neurons (i.e. GABAergic or glutamatergic), it may well be that some of the putative high firing neurons are inhibitory neurons. Previous studies have shown that GABAergic neurons show high firing rates in vivo (Gentet et al., 2010; Mateo et al., 2011). This in turn would support more the second coding strategy, where a larger population of low firing neurons (putatively projecting neurons) has to be read out by a downstream region to create a stable percept of the stimulus. Furthermore, we cannot exclude the possibility that supragranular neurons are not required for decoding different whisker stimuli (Constantinople and Bruno, 2013).

Since only a small population is highly active and a large number of neurons remain silent (30%), there is a large resource for plasticity (Brecht et al., 2005; Kerr et al., 2007; Lütcke et al., 2013; Margolis et al., 2012). Upon sensory deprivation, there is functional reorganization in the corresponding somatosensory cortex (Diamond et al., 1994; Feldman, 2005; Margolis et al., 2012). Following whisker trimming, responses evoked by stimulation of the trimmed whisker are reduced after only one day. Neurons in the supragranular and infragranular layers respond rapidly to changes in sensory experience. Adding (i.e. from the large pool of silent cells) or removing a few neurons (i.e. from high responding neurons) will lead to a large relative change in the evoked activity and may have a dramatic effect on the behavior of the animal (Houweling and Brecht, 2007).

Conclusions

Our main finding is a remarkable stability of cortical whisker stimulus representation at the single-cell and population level over many weeks, governed by a small population of highly active neurons. The observed map conservation in neuronal ensembles led by a small set of highly responsive neurons could be a building block for reliable and stable representation of sensory percepts seen in trained animals.

Acknowledgments

We thank Wolfger von der Behrens, Simon Musall, Renaud Jolivet, and Jill Stobart for comments on an earlier version of the manuscript. We also thank Stefan Weber for technical assistance. This work was supported by the EU-FP7 program (BRAIN-I-NETS project 243914 and BrainScales project 269921 to F.Ha. and F.He.), the Swiss National Science Foundation (grant PP00B-110751/1 to B.W.), the Faculty of Medicine at the RWTH Aachen University (grant from the Interdisciplinary Center for Clinical Research (IZKF Aachen) to F.Ha.), and SystemsX.ch (NEUROCHOICE 51RT-0_145732) (project 2008/2011-Neurochoice to F.He. and B.W.). B.W. is a member of the Clinical Research Priority Program "Molecular Imaging Network Zurich". The authors declare no competing financial interests.

References

Adibi, M., Diamond, M.E., Arabzadeh, E., 2012. Behavioral study of whisker-mediated vibration sensation in rats. Proc. Natl. Acad. Sci. 109, 971–976.

Andermann, M.L., Ritt, J., Neimark, M.A., Moore, C.I., 2004. Neural correlates of vibrissa resonance-band-pass and somatotopic representation of high-frequency stimuli. Neuron 42, 451–464.

Arabzadeh, E., Petersen, R.S., Diamond, M.E., 2003. Encoding of whisker vibration by rat barrel cortex neurons: implications for texture discrimination. J. Neurosci. 23, 9146–9154.

Arabzadeh, E., Zorzin, E., Diamond, M.E., 2005. Neuronal encoding of texture in the whisker sensory pathway. PLoS Biol. 3, e17.

Barth, A.L., Poulet, J.F.A., 2012. Experimental evidence for sparse firing in the neocortex. Trends Neurosci. 35, 345–355.

Bathellier, B., Ushakova, L., Rumpel, S., 2012. Discrete neocortical dynamics predict behavioral categorization of sounds. Neuron 76, 435–449.

Bellavance, M.-A., Demers, M., Deschenes, M., 2010. Feedforward inhibition determines the angular tuning of vibrissal responses in the principal trigeminal nucleus. J. Neurosci. 30, 1057–1063.

Brecht, M., Schneider, M., Manns, I.D., 2005. Silent neurons in sensorimotor cortices: implications for cortical plasticity. In: Ebner, F. (Ed.), Neural Plasticity in Adult Somatic Sensory-motor Systems. CRC Press, Boca Raton, FL, pp. 1–19.

Carvell, G., Simons, D., 1990. Biometric analyses of vibrissal tactile discrimination in the rat. J. Neurosci. 10, 2638–2648.

Cetin, A., Komai, S., Eliava, M., Seeburg, P.H., Osten, P., 2007. Stereotaxic gene delivery in the rodent brain. Nat. Protoc. 1, 3166–3173.

Chang, C.-C., Lin, C.-J., 2011. LIBSVM: a library for support vector machines. ACM Trans. Intell. Syst. Technol. (TIST) 2, 27.

Chen, J.L., Carta, S., Soldado-Magraner, J., Schneider, B.L., Helmchen, F., 2013. Behaviour-dependent recruitment of long-range projection neurons in somatosensory cortex. Nature 499, 336–340.

Cohen, L., Koffman, N., Meiri, H., Yarom, Y., Lampl, I., Mizrahi, A., 2013. Time-lapse electrical recordings of single neurons from the mouse neocortex. Proc. Natl. Acad. Sci. 110, 5665–5670.

Constantinople, C.M., Bruno, R.M., 2013. Deep cortical layers are activated directly by thalamus. Science 340, 1591–1594.

Crochet, S., Poulet, J.F.A., Kremer, Y., Petersen, C.C.H., 2011. Synaptic mechanisms underlying sparse coding of active touch. Neuron 69, 1160–1175.

Diamond, M.E., Huang, W., Ebner, F.F., 1994. Laminar comparison of somatosensory cortical plasticity. Science 265, 1885–1888.

Ewert, T.A.S., Vahle-Hinz, C., Engel, A.K., 2008. High-frequency whisker vibration is encoded by phase-locked responses of neurons in the rat's barrel cortex. J. Neurosci. 28, 5359–5368.

Feldman, D.E., 2005. Map plasticity in somatosensory cortex. Science 310, 810–815.

Gentet, L.J., Avermann, M., Matyas, F., Staiger, J.F., Petersen, C.C.H., 2010. Membrane potential dynamics of GABAergic neurons in the barrel cortex of behaving mice. Neuron 65, 422–435.

Gerdjikov, T.V., Bergner, C.G., Stüttgen, M.C., Waiblinger, C., Schwarz, C., 2010. Discrimination of vibrotactile stimuli in the rat whisker system: behavior and neurometrics. Neuron 65, 530–540.

Helmchen, F., Imoto, K., Sakmann, B., 1996. Ca^{2+} buffering and action potential-evoked Ca^{2+} signaling in dendrites of pyramidal neurons. Biophys. J. 70, 1069–1081.

Hernández, A., Zainos, A., Romo, R., 2000. Neuronal correlates of sensory discrimination in the somatosensory cortex. Proc. Natl. Acad. Sci. 97, 6191–6196.

Houweling, A.R., Brecht, M., 2007. Behavioural report of single neuron stimulation in somatosensory cortex. Nature 451, 65–68.

Huber, D., Petreanu, L., Ghitani, N., Ranade, S., Hromádka, T., Mainen, Z., Svoboda, K., 2008. Sparse optical microstimulation in barrel cortex drives learned behaviour in freely moving mice. Nature 451, 61–64.

Hutson, K.A., Masterton, R.B., 1986. The sensory contribution of a single vibrissa's cortical barrel. J. Neurophysiol. 56, 1196–1223.

Jadhav, S.P., Wolfe, J., Feldman, D.E., 2009. Sparse temporal coding of elementary tactile features during active whisker sensation. Nat. Neurosci. 12, 792–800.

Jenkinson, E.W., Glickstein, M., 2000. Whiskers, barrels, and cortical efferent pathways in gap crossing by rats. J. Neurophysiol. 84, 1781–1789.

Kerr, J.N.D., de Kock, C.P.J., Greenberg, D.S., Bruno, R.M., Sakmann, B., Helmchen, F., 2007. Spatial organization of neuronal population responses in layer 2/3 of rat barrel cortex. J. Neurosci. 27, 13316–13328.

Khatri, V., 2004. Adaptation in thalamic barreloid and cortical barrel neurons to periodic whisker deflections varying in frequency and velocity. J. Neurophysiol. 92, 3244–3254.

Knutsen, P.M., 2006. Haptic object localization in the vibrissal system: behavior and performance. J. Neurosci. 26, 8451–8464.

Langer, D., van't Hoff, M., Keller, A.J., Nagaraja, C., Pfäffli, O.A., Göldi, M., Kasper, H., Helmchen, F., 2013. HelioScan: a software framework for controlling in vivo microscopy setups with high hardware flexibility, functional diversity and extendibility. J. Neurosci. Methods 215, 38–52.

Lefort, S., Tomm, C., Floyd Sarria, J.-C., Petersen, C.C.H., 2009. The excitatory neuronal network of the C2 barrel column in mouse primary somatosensory cortex. Neuron 61, 301–316.

Li, L., Ebner, F.F., 2007. Cortical modulation of spatial and angular tuning maps in the rat thalamus. J. Neurosci. 27, 167–179.

Lottem, E., Azouz, R., 2009. Mechanisms of tactile information transmission through whisker vibrations. J. Neurosci. 29, 11686–11697.

Luna, R., Hernández, A., Brody, C.D., Romo, R., 2005. Neural codes for perceptual discrimination in primary somatosensory cortex. Nat. Neurosci. 8, 1210–1219.

Lütcke, H., 2010. Optical recording of neuronal activity with a genetically-encoded calcium indicator in anesthetized and freely moving mice. Front. Neural Circ. 4 (9), 1–12.

Lütcke, H., Margolis, D.J., Helmchen, F., 2013. Steady or changing? Long-term monitoring of neuronal population activity. Trends Neurosci. 36, 375–384.

Margolis, D.J., Lütcke, H., Schulz, K., Haiss, F., Weber, B., Kügler, S., Hasan, M.T., Helmchen, F., 2012. Reorganization of cortical population activity imaged throughout long-term sensory deprivation. Nat. Neurosci. 15, 1539–1546.

Masino, S.A., Frostig, R.D., 1996. Quantitative long-term imaging of the functional representation of a whisker in rat barrel cortex. Proc. Natl. Acad. Sci. 93, 4942–4947.

Mastakov, M., 2001. Combined injection of rAAV with mannitol enhances gene expression in the rat brain. Mol. Ther. 3, 225–232.

Mateo, C., Avermann, M., Gentet, L.J., Zhang, F., Deisseroth, K., Petersen, C.C.H., 2011. In vivo optogenetic stimulation of neocortical excitatory neurons drives brain-state-dependent inhibition. Curr. Biol. 21, 1593–1602.

Mayrhofer, J.M., Skreb, V., von der Behrens, W., Musall, S., Weber, B., Haiss, F., 2013. Novel two-alternative forced choice paradigm for bilateral vibrotactile whisker frequency discrimination in head-fixed mice and rats. J. Neurophysiol. 109, 273–284.

McMahon, D.B.T., Jones, A.P., Bondar, I.V., Leopold, D.A., 2014. Face-selective neurons maintain consistent visual responses across months. Proc. Natl. Acad. Sci. 111, 8251–8256.

Mehta, S.B., Whitmer, D., Figueroa, R., Williams, B.A., Kleinfeld, D., 2007. Active spatial perception in the vibrissa scanning sensorimotor system. PLoS Biol. 5, e15.

Melzer, P., Sachdev, R.N.S., Jenkinson, N., Ebner, F.F., 2006. Stimulus frequency processing in awake rat barrel cortex. J. Neurosci. 26, 12198–12205.

Minderer, M., Liu, W., Sumanovski, L.T., Kügler, S., Helmchen, F., Margolis, D.J., 2011. Chronic imaging of cortical sensory map dynamics using a genetically encoded calcium indicator. J. Physiol. 590, 99–107 (no–no).

Moore, C.I., 2004. Frequency-dependent processing in the vibrissa sensory system. J. Neurophysiol. 91, 2390–2399.

Morita, T., Kang, H., Wolfe, J., Jadhav, S.P., Feldman, D.E., 2011. Psychometric curve and behavioral strategies for whisker-based texture discrimination in rats. PLoS ONE 6, e20437.

Musall, S., von der Behrens, W., Mayrhofer, J.M., Weber, B., Helmchen, F., Haiss, F., 2014. Tactile frequency discrimination is enhanced by circumventing neocortical adaptation. Nat. Neurosci. 17, 1567–1573.

Niessing, J., Friedrich, R.W., 2010. Olfactory pattern classification by discrete neuronal network states. Nature 465, 47–52.

O'Connor, D.H., Peron, S.P., Huber, D., Svoboda, K., 2010. Neural activity in barrel cortex underlying vibrissa-based object localization in mice. Neuron 67, 1048–1061.

Olshausen, B., Field, D., 2004. Sparse coding of sensory inputs. Curr. Opin. Neurobiol. 14, 481–487.

Petersen, C.C.H., Crochet, S., 2013. Synaptic computation and sensory processing in neocortical layer 2/3. Neuron 78, 28–48.

Pologruto, T.A., Sabatini, B.L., Svoboda, K., 2003. ScanImage: flexible software for operating laser scanning microscopes. Biomed. Eng. Online 2, 13.

Safaai, H., von Heimendahl, M., Sorando, J.M., Diamond, M.E., Maravall, M., 2013. Coordinated population activity underlying texture discrimination in rat barrel cortex. J. Neurosci. 33, 5843–5855.

Salinas, E., Hernandez, A., Zainos, A., Romo, R., 2000. Periodicity and firing rate as candidate neural codes for the frequency of vibrotactile stimuli. J. Neurosci. 20, 5503–5515.

Shuler, M.G., Krupa, D.J., Nicolelis, M.A.L., 2001. Bilateral integration of whisker information in the primary somatosensory cortex of rats. J. Neurosci. 21, 5251–5261.

Srivastava, V., Parker, D.J., Edwards, S.F., 2008. The nervous system might "orthogonalize" to discriminate. J. Theor. Biol. 253, 514–517.

Stüttgen, M.C., Schwarz, C., 2010. Integration of vibrotactile signals for whisker-related perception in rats is governed by short time constants: comparison of neurometric and psychometric detection performance. J. Neurosci. 30, 2060–2069.

Tsytsarev, V., Pope, D., Pumbo, E., Yablonskii, A., Hofmann, M., 2010. Study of the cortical representation of whisker directional deflection using voltage-sensitive dye optical imaging. NeuroImage 53, 233–238.

Von Heimendahl, M., Itskov, P.M., Arabzadeh, E., Diamond, M.E., 2007. Neuronal activity in rat barrel cortex underlying texture discrimination. PLoS Biol. 5, e305.

Wiest, M.C., 2005. Heterogeneous integration of bilateral whisker signals by neurons in primary somatosensory cortex of awake rats. J. Neurophysiol. 93, 2966–2973.

Wolfe, J., Hill, D.N., Pahlavan, S., Drew, P.J., Kleinfeld, D., Feldman, D.E., 2008. Texture coding in the rat whisker system: slip-stick versus differential resonance. PLoS Biol. 6, e215.

Yassin, L., Benedetti, B.L., Jouhanneau, J.-S., Wen, J.A., Poulet, J.F.A., Barth, A.L., 2010. An embedded subnetwork of highly active neurons in the neocortex. Neuron 68, 1043–1050.